Low-Dispersion Electrokinetic Flows for Expanded Separation Channels in Microfluidic Systems: Multiple Faceted Interfaces

Gregory J. Fiechtner and Eric B. Cummings*

Sandia National Laboratories, P.O. Box 969, MS 9951, Livermore, California 94550

Submitted to *Journal of Chromatography A*

In Press (September, 2003)

*Corresponding author. E-mail: gjfiech@sandia.gov, Tel: 925-294-3161, Fax: 925-294-3020

Low-Dispersion Electrokinetic Flows for Expanded Separation Channels in Microfluidic Systems: Multiple Faceted Interfaces

Gregory J. Fiechtner and Eric B. Cummings*

Sandia National Laboratories, P.O. Box 969, MS 9951, Livermore, California 94550

*Corresponding author. E-mail: gjfiech@sandia.gov, Tel: 925-294-3161, Fax: 925-294-3020

Abstract

A novel methodology to design on-chip conduction channels is presented for expansion of low-dispersion separation channels. Designs are examined using two-dimensional numerical solutions of the Laplace equation with a Monte Carlo technique to model diffusion. The design technique relies on trigonometric relations that apply for ideal electrokinetic flows. Flows are rotated and stretched along the abrupt interface between adjacent regions having differing specific permeability. Multiple interfaces can be placed in series along a channel. The resulting channels can be expanded to extreme widths while minimizing dispersion of injected analyte bands. These channels can provide a long path length for line-of-sight optical absorption measurements. Expanded sections can be reduced to enable point detection at the exit section of the channel. Designed to be shallow, these channels have extreme aspect ratios in the wide section, greatly increasing the surface-to-volume ratio to increase heat removal and decrease unwanted pressure-driven flow. The use of multiple interfaces is demonstrated by considering several three-interface designs. Faceted flow splitters can be constructed to divide channels into any number of exit channels while minimizing dispersion. The resulting manifolds can be used to construct medians for structural support in wide, shallow channels.

Keywords

Electrochromatography; Electrophoresis; Electrokinesis; Facet; Separations; Chips; Chromatography; Dispersion; Microchips; Microfluids; Electrokinetic Flows; Band Spreading

1. Introduction

Flow-field dimensions are an important consideration in capillary electrophoresis. Tube diameter and shape impact Joule heating, siphoning, and detection. Use of capillaries with comparatively small diameters increases heat removal to the capillary walls by increasing surface-to-volume ratio [1-8]. Capillaries can also be designed with "bubble cells" to increase the absorption pathlength for detection after expanding the flow from the injection and separation regions of the capillary [9-11]. The use of square capillaries has been found to reduce the impact of Joule heating [12-17], and they can be designed for an optimum aspect ratio based on diffusion [18]. Square capillaries can be implemented to improve detection limits for optical absorption measurements [16]. Microfluidic, chip-based systems have received considerable attention in an effort to miniaturize instruments based on capillary electrophoresis. Here, the chip substrate increases the capacity to sink heat when compared to capillaries [19], such that comparatively large voltages can be applied while maintaining Joule heating effects at an acceptable level [20-23]. Nevertheless, Joule heating can still negatively influence separation results for a given channel width, particularly as channel depth is increased [24, 25]. Moreover, common microchannel structures—such as T-shaped or multi-branched circuits—can also exhibit temperature gradients caused by Joule heating [26]. As the size of capillaries and channels is decreased, the volumetric flowrate of pressure-induced flows from siphoning will decrease with hydraulic radius to the fourth power, while that for electrokinetic flow will decrease with radius squared. Thus, the ratio of the electrokinetic to the pressure-driven flowrate is inversely proportional to the radius squared [27]. Consequently, unwanted band broadening caused by siphoning [5, 28-30] will decrease for small channels. Moreover, the resistance to pressure driven flow increases as channel

dimensions are decreased (and the surface-to-volume ratio is increased) owing to electro-viscous coupling in the electric double layer [31-35].

Wide, shallow channels offer many practical advantages for microfluidic systems. The delivery of light to chip-based systems using waveguides and optical fibers has been the subject of numerous investigations [25, 36-50]. As light delivery and collection from chip-based detectors become routine, channel designs that optimize the delivery of samples for optical detection will be an important feature. To this end, wide channels are advantageous for on-chip absorption detection because they maximize the optical path length. In particular, shallow channels enable the use of evanescent excitation with a larger fraction of analyte being delivered in proximity of the incident light. While important for optical detection, channels that are both wide and shallow offer further advantages to chip-based instruments. Shallow channels minimize the time for molecules to diffuse to channel walls—advantageous for assays and open-channel electrochromatography.

Clearly, channel dimensions and shape can be an important consideration for capillary electrophoresis. In this paper, we introduce a novel method that offers several potential advantages over capillary systems and conventional, microchip-based systems. The technique expands channels while retaining a flat velocity profile afforded by electrokinetic flow. The channels can be expanded from inlets with more modest aspect ratios, enabling their use with conventional microfluidic sample-injection methods [5, 20, 28, 51-55].

1.1 Dispersion in Electrokinetic Flows

Electrokinetic pumping is an attractive method for sample handling, and this technique has led to a large number of studies that examine the consequences of the design of channels on analyte dispersion in electrokinetic flows. Low-dispersion turns were developed during these past studies, in part, to place a long separation column into a high-density fluidic circuit. Most of these low-dispersion designs are predicated on reducing the “racetrack effect” that results from the shorter path length on the inside wall of a turn compared to that for the outside wall, complicated further by the corresponding distribution of

the electric-field strength [56]. Because comparatively narrow channels minimize this effect, a number of designs incorporate turning sections that are narrower than the straight sections of conduction channel [36, 37, 57-68]. Alternatively, designs can minimize the dispersion by altering the channel geometry immediately after the turning section [69]. The racetrack effect is also reduced greatly by using turns for which the radius of curvature is large compared to the channel width [70-73]. Complementary pairs of turns can reduce the dispersion introduced using a single turn [73]. Wavy walls on the inner side of turns reduce the flow velocity there with respect to that for the outer wall [74]. The velocity on a channel sidewall of a polymer microchannel can be increased by pre-treating the wall with a pulsed, UV laser, thereby decreasing dispersion in turns[75, 76]. In addition to turns, expansion of capillary flows to wide bubble cells has been demonstrated to increase dispersion [9]. The novel designs proposed in our paper both turn and expand flows while minimizing dispersion.

1.2 Faceted Design Method

In a prior study, we introduced a new "faceted" design methodology that implements results from the theory of ideal electrokinetic flows [77]. Rather than address the racetrack effect directly, the technique uses abrupt changes in channel cross-sectional area along lines of distinct angle to affect a flow system having a piecewise uniform velocity. Two lines ("interfaces") of abrupt transition in cross sectional area are designed to enclose faceted "prisms"—terminology that is explained below—which are characterized by uniform velocity, and exhibit straight and parallel streaklines. Faceted prisms can be placed in series to generate turns of nearly any angle and width. The resulting technique allows the use of simple trigonometric relations to calculate the design parameters, enabling the algebraic optimization and dispersion minimization of electrokinetic-channel designs.

Faceted prisms inherently employ designs that are optimized for two-interface systems. While prisms can be placed in series to construct wide channels, an alternative approach is to design expanded channels by coordinating a sequence of multiple interfaces. The simultaneous mathematical treatment of numerous interfaces affords greater flexibility in choosing design constraints. The penalty is that simple

trigonometric expressions cannot always be obtained, with the design process requiring iterative solutions of simultaneous trigonometric equations. Nevertheless, these solutions are obtained readily using inexpensive commercial software on a personal computer. Moreover, the use of multiple interfaces can produce turns and expansions of extreme size. For example, systems of seven interfaces placed in series can be selected to produce spiraled turns of over 400 degrees with expansion factors of over 1000. To illustrate the design of channels for electrokinetic flows using multiple interfaces, we present results for three-interface systems.

The design of flow splitters and manifolds is also considered in this paper using faceted interface designs. Such flow splitters enable on-chip implementation of multiple-dimension separations using a single analyte injection. Faceted interfaces can be used to design simple flow splitters for applications such as electrokinetically driven T-sensors [78], H-filters [79, 80], T-junctions [81], dilution junctions [82], or for manifolds to split flow into large numbers of channels [83]. When implemented with expanding channels, splitters can be used to increase the degree of channel expansion. When implemented with parallel flow displacers, manifolds can be used to place large numbers of parallel channels within a multi-interface expander. The resulting parallel structure can be used to minimize the degree of transverse diffusion [18] and provide structural support for bonded channel covers [84].

1.3 Overview

Following an introduction to the faceted design equations, results for three-interface expanders are presented. Direct numerical simulation of electrokinetic flows requires solution of the Navier-Stokes, species transport, and electric field equations that are coupled through the charge density, which is generally unknown. Moreover, the relevant length scales typically span ~7 orders of magnitude. Fortunately, "similitude" exists for most cases of interest, such that the velocity field can be computed directly from the Laplace equation without the need to solve the continuity and momentum equations [85]. Therefore, in this paper, designs are demonstrated computationally using two-dimensional numerical solutions of the Laplace equation [86]. A Monte Carlo method is used to demonstrate the

influence of diffusion, which is reported using the dimensionless Peclet number [77]. Novel methods to split flows are then shown, including the use of manifolds as support structures in wide, shallow separation columns. Expansions are considered for comparatively small Peclet numbers—corresponding to a large amount of diffusion—showing that three-interface systems can result in a linearly varying, cumulative amount of diffusion across a channel.

2. Theory

For a single faceted interface, "permeability", having dimensions of area, represents the cross-sectional area of the channel at each side of the interface. However, it is the *specific* permeability, σ_{sp}—having dimemsions of length—that is chosen on each side of an interface using the faceted technique [77]. For a system of channels limited to two distinct etch depths, the specific permeability is chosen to have either of two values. To analyze steady fluid conduction past an abrupt change in specific permeability, we consider the conduction channel sketched in Fig. 1, having a uniform specific permeability σ_{sp1} (m^2) in Region 1, left of a line of transition, Interface 1, and a uniform specific permeability σ_{sp2} in Region 2, right of Interface 1. For a multi-interface system, care must be taken with this terminology. A two-interface system using a two-level etch has an inlet specific permeability of σ_{sp1} followed by a prism with specific permeability σ_{sp2}, and an exit Region 3 with a specific permeability of σ_{sp1}, as illustrated in Fig. 1(a). Although the specific permeabilities—and thus the depths—of the entrance and exit are identical, the corresponding cross-sectional areas in Regions 1 and 3 need not be equal.

Several methods can be employed to modify the specific permeability of a channel. In a quasi-planar channel, the specific permeability is proportional to the channel depth, which can be changed abruptly at an interface using a two-level etch. Alternatively, specific permeability can be lowered with respect to an open channel by blocking part of the channel, for example, by filling the channel with an array of posts or channel-aligned parallel columns. Additionally, the channel can be filled with a packing or porous medium or pores can be generated in the substrate. For the channel designs discussed in this

paper, the abrupt change in specific permeability will always occur along a line, with the angle of the line with respect to the walls being chosen from a range of values. Each method for changing the specific permeability generates characteristic levels of hydrodynamic dispersion at the interface and throughout the conduction channel and can be used separately or in combination.

The design rules used to describe flow passing across an abrupt change in specific permeability result from the theory of ideal electrokinetic flow. Similitude applies under the following conditions [85]:

1. The electric field is steady;
2. fluid properties are uniform;
3. channel boundaries are uniform, insulating, and impermeable;
4. the electric Debye layer is thin compared to any physical dimension; and
5. fluid velocities on all inlet and outlet boundaries satisfy the Helmholtz-Smoluchowski relation normally applicable to fluid-solid boundaries.

For these conditions, the velocity $\mathbf{u}$ (m s^{-1}) of the conduction fluid is everywhere proportional to the electric field $\mathbf{E}$ (V m^{-1}) such that

$$\mathbf{u}=\mu\mathbf{E}, \tag{1}$$

where the coefficient μ (m^2 V^{-1} s^{-1}) is the mobility of the fluid. The mobility and the fluid conductivity are assumed to be constant everywhere.

For an insulating substrate containing an electrokinetic flow, the corresponding tangential electric field is not changed by the interface. Therefore, application of conditions of similitude along with the conservation of mass results in two equations and two unknowns. These can be solved to obtain the "compatibility relationship" given by [77]

$$\frac{\tan\theta_1}{\sigma_{sp1}}=\frac{\tan\theta_2}{\sigma_{sp2}}, \tag{2}$$

where θ_1 and θ_2 are the flow angles shown in Fig. 1 (a). Channels designed to satisfy Eq. (2) exhibit uniform speed on each side of the interface given by

$$u_{10}\sin\theta_1 = u_{20}\sin\theta_2, \tag{3}$$

where $u \equiv \|\mathbf{u}\|$ and and $\mathbf{u}_{1o}$ and $\mathbf{u}_{2o}$ (m s^{-1}) are the velocities before and after Interface 1, respectively. The widths w_1 and w_2 of the conduction channels in Region 1 and Region 2 in Fig. 1 (a) obey the relation

$$\frac{w_1}{\cos\theta_1} = \frac{w_2}{\cos\theta_2}. \tag{4}$$

Here, the expansion ratio for Interface 1 is defined as w_2/w_1. The channel turns the flow velocity at Interface 1 by an amount equal to $\theta_1 - \theta_2$.

The motion of material lines through a channel is often of interest. For example, if a volume of analyte is injected into an electrokinetic flow for purposes of separation, the line formed by the leading edge of the injected band defines a "material line", and the degree of distortion of this line as it travels through a system of conduction channels is of critical importance. The material lines are rotated exclusively at the interface between regions of distinct specific permeability. This rotation is depicted in Fig. 1 (b), where the dashed line represents the material line, which is shown at six distinct instances of time—t_1, t_2, t_3, t_4, t_5 and t_6—as it propagates through a channel. The material-line angles ψ_1 and ψ_2 are formed between the direction of flow and the normal to the material line for Region 1 and Region 2, respectively. The resulting trigonometric relationships can be arranged to obtain

$$\tan\psi_2 = (\sigma_{sp1}/\sigma_{sp2}) \cos^2\theta_1 [\tan\psi_1 + \tan\theta_1 (1 - (\sigma_{sp2}/\sigma_{sp1})^2 (1 - \tan\psi_1\tan\theta_1))]. \tag{5}$$

At instant t_3, the band bends abruptly at Interface 1, similar to the refraction of light. Indeed, Eq. (2) is similar in appearance to Snell's law of refraction, except that tangents of the propagation angles are matched instead of sines. For this reason, we refer to a design element bounded by two interfaces as a faceted "prism".

So far, the flow past Interface 1 in Fig. 1 has been considered. The second abrupt change in permeability, denoted by Interface 2, forms the downstream boundary of Region 2. This labeling convention is based on the occurrence of both an incidence and exit angle for each interface, denoted by θ_{21} and θ_{22} for Interface 2. The illustration of Fig. 1 depicts a pair of interfaces. For a three-interface

system, each interface turns the flow, such that the overall turning angle is defined using the turning angles for each interface:

$$\theta_{\mathrm{T}} = (\theta_2 - \theta_1) + (\theta_{22} - \theta_{21}) + (\theta_{32} - \theta_{31}) + \cdots. \tag{6}$$

2.1 Two-Interface Systems

A common design goal is a device that produces no net rotation or skew of material lines with respect to the flow direction. Any single, non-trivial interface having a non-zero incidence angle skews material lines with respect to the flow. However, if the material line is perpendicular to the flow direction initially, then $\psi_1 = 0$, and Eq. (5) simplifies to [77]

$$\tan\psi_2\big|_{\psi_1=0} = \left(\frac{\sigma_{\mathrm{sp1}}}{\sigma_{\mathrm{sp2}}} - \frac{\sigma_{\mathrm{sp2}}}{\sigma_{\mathrm{sp1}}}\right)\frac{\sin 2\theta_1}{2}. \tag{7}$$

Equation (7) is symmetric about θ_1=45°, yielding two cases that eliminate skew of material lines at the exit of a two-interface system: If the exit angle of the second interface is given by $\theta_{22} = 90° - \theta_1$, the resulting channel rotates the flow and expands or contracts the width. The resulting turning angle is given by

$$\theta_{\mathrm{T}} = \frac{\pi}{2} - 2\theta_1 + \tan^{-1}\left(\frac{\sigma_{\mathrm{sp2}}}{\sigma_{\mathrm{sp1}}}\tan\theta_1\right) - \tan^{-1}\left(\frac{\sigma_{\mathrm{sp2}}}{\sigma_{\mathrm{sp1}}}\frac{1}{\tan\theta_1}\right). \tag{8}$$

The expansion ratio of a device having back-to-back interfaces is equal to the quotient of the width ratios at the larger and smaller incidence angles. The corresponding width ratio for a skew-compensated two-interface pair is given by the expression

$$\frac{w_1}{w_4} = \frac{\sigma_{\mathrm{sp1}}}{\sigma_{\mathrm{sp2}}}\sqrt{\frac{1 + \left(\frac{\sigma_{\mathrm{sp2}}}{\sigma_{\mathrm{sp1}}}\right)^2 (\tan\theta_1)^2}{1 + \left(\frac{\sigma_{\mathrm{sp1}}}{\sigma_{\mathrm{sp2}}}\right)^2 (\tan\theta_1)^2}}. \tag{8}$$

The width ratio has a maximum value of $\sigma_{sp1}/\sigma_{sp2}$. For the condition $\theta_{22} = \theta_1$ the turning angle, θ_Γ, is zero for all incidence angles, and the width is identical for the entrance and exit of the channel. The resulting channel designs are flow displacers that do not rotate or expand the flow.

2.2 Three-Interface Systems

As here envisioned, on-chip separation channels would likely use a deep section for sample injection, and a wide, shallow separation column. A single interface can expand a flow and change the channel depth from but cannot compensate skew. A two-interface system has identical specific permeabilities at the inlet and exit; therefore, a two-level etch will result in identical depths for both inlet and outlet sections. A system with two specific permeabilities requires at least three interfaces to compensate skew and provide different depths. The third interface adds one degree of freedom to the skew-compensation problem: given one interface, the two other interfaces can be adjusted in concert over a range of angles to compensate or control skew. This additional degree of freedom is useful, for example, to produce skew-controlled designs that produce a prescribed flow turning angle or the maximum expansion factor.

A faceted interface system that expands a narrow, deep channel into a wide, shallow channel is useful for open-channel electrochromatography. A three-interface system to perform this expansion will use large incidence angles for the first and third interfaces to expand the channel and the smallest possible incidence angle for the second interface to compensate skew while contracting the channel minimally. The largest allowable incidence angle ($|\theta_{1max}| < 90°$) depends on design constraints and fabrication limits. Assuming the allowable angle does not depend on channel width, an optimal three-interface system will set the first and third interface angles, respectively, to $+\theta_{1max}$ and $-\theta_{1max}$. The sign of the angle describes the relative orientation of the interfaces. This opposing orientation is chosen because it partly compensates skew.

Setting the incidence angles in this fashion removes the extra degree of freedom in the system, constraining the angle of the second interface to isolated solutions of a transcendental equation. Figure 2 contains plots at various specific-permeability ratios of the minimum skew-compensating incidence

angle of the second interface obtained by solving this transcendental equation as a function of the magnitude of the first and third incidence angles. The expanded plot in Fig. 2 (b) shows the solutions in the practically important range of angles 80-90°. The maximum expansion of the three-interface system occurs when the angle of the internal interface is zero, producing no contraction of the channel. The solutions for this angle approach zero as the magnitude of the first and third incidence angle approaches 90°. However, the peak value of the internal angle also occurs near 90°, particularly at large specific-permeability ratios. Practical systems may not benefit from this dip in the internal angle because of the extreme incidence angles required.

Figure 3 (a) shows the resulting expansion ratio of the skew-compensating, three-interface system. As the magnitudes of the first and third incidence angles approach 90°, the expansion ratio approaches the theoretical maximum, $(\sigma_{sp1}/\sigma_{sp2})^2$. The expansion ratio drops precipitously away from 90°, such that much lower ratios are likely to be realized in practice. Figure 3 (b) shows the ratio of the expansion factor of the three-interface system to that of the first (or third) interface. In the evident plateau region (at a ratio around 1.7) for larger permeability ratios (~10 and above), the contraction across the second interface largely overcomes the additional expansion from the third (or first) interface, such that the overall expansion is less than a factor of two higher than that of a single-interface expansion.

Figure 4 shows the turning angle of the skew-compensating, three-interface system. The first and third angles are arranged oppositely so their turning angles cancel each other. Flow turning is therefore dominated by the second interface. Plots such as those shown in Figs. (2)-(4) illustrate that, although an iterative solution to simultaneous equations for each interface is necessary for three-interface systems, it is still straightforward to obtain a domain of design parameters that is easy to compute and visualize. Some examples of three-interface designs will now be demonstrated using numerical solutions of the Laplace equation with a Monte Carlo treatment of diffusion.

3. Results and discussion

3.1 Three-Interface Expanders

Figure 5 show numerical simulations of flow in a three-interface, skew-compensated system. The permeability ratio is 10, and the maximum incidence angle is 85°. The expansion factor for the compensated system is 14.32, which is approximately 1.9 times larger than that for the single-interface expansion factor. The incidence angle of the second interface (θ_{21}) is 22.82°. The substrate is depicted by the gray background. The black arrows along the top edge of the channel in Fig. 5 (a) show the flow direction in each faceted prism. Since the interfaces were designed to satisfy the compatibility condition, the velocity in each prism is uniform. Therefore, the numerical solution results in a uniform color for each faceted prism, with the relative speed given by the color table in the upper left corner of the image. Because the velocity is uniform in each section, the resulting streaklines are straight and parallel—except at an interface, where they are turned abruptly. Recent experimental visualization of particle paths in faceted prisms has confirmed this behavior [87]. A band is injected into the channel at time t_1 in Fig 5 (b) with no skew with respect to the flow direction. When the band is traveling in two faceted prisms, as shown at instances t_2, t_3, t_4, and t_5, it bends abruptly at an interface, but it remains straight within the prisms. The band is rotated when traveling through the second and third prisms, but the skew is removed completely as the band enters the fourth channel section. For a 100-μm entrance, the optical path across the channel between an incident laser beam and a photodetector as shown will be 1.43 mm. The band broadening shown in Fig. 5 (b) was computed assuming a Peclet number at the channel inlet of 402. Because the velocity in each faceted prism is uniform, the Peclet number is uniform in each region and is proportional to the local velocity. For example, the Peclet number in Region 3 is 163.

If we instead hold the incidence angle of the second interface to a value of 0°, an uncompensated, three-interface system results. That is, bands that enter the channel perpendicular to the flow direction will pass through the exit section with a finite rotation angle. In this case, the uncompensated system will have the same maximum incidence angle, resulting in an expansion factor of ~ 57.08 (the square of

the single-interface expansion factor). The skew of the uncompensated three-interface system produces a net broadening increase because of transverse diffusion. The material-line tilt angle along the expanded channel is $\psi \simeq 40.18°$. The material line is longer by a factor of $1/\cos\psi \simeq 1.31$ than an un-skewed line. The stretching of the line also sharpens gradients normal to the material line by a corresponding amount so diffusion produces $1/\cos^2\psi \simeq 1.71$x more transport normal to the skewed material line than an un-skewed line. This degradation in performance may be offset by other factors or design considerations that favor an uncompensated or partly compensated three-interface system.

An example of a three-interface system without skew compensation is shown in Fig. 6. For a system with a maximum incidence angle of 85°, the large degree of expansion results in a computational grid that is extremely large. Consequently, the memory of the personal computer was not sufficient to solve for the channel flow field with a reasonable grid resolution. Therefore, a similar channel expander was designed using an incidence angle for the first interface that was reduced to 81.17°. Here, the expansion ratio is 30, and the material-line angle of the band in the final channel section is 55.44°. The rotated band increases the amount of transverse diffusion, but for optical absorption measurements, the rotation results in a longer absorption path. For a maximum incidence angle of 85° for interface 1, and assuming an inlet channel width of 100 μm, the optical absorption path length will be 7.48 mm. Therefore, an uncompensated three-interface system with an identical incidence angle as that for a skew-compensated three-interface system will increase the absorption path length significantly. For a maximum incidence angle of 85°, the path length for absorption of light is increased by a factor of 5.22. This does not mean that the amount of light absorbed will be increased by the same factor—the sample concentration is unchanged in an ideal electrokinetic flow, and the analyte band is stretched to a wide, shallow plug, such that signal increase could result primarily from matching band shape to the laser profile. Moreover, for such extreme channel widths, light divergence upon exiting a waveguide might decrease signal levels appreciably.

For extreme channel widths, sagging of the channel cover might occur. As a result, the channel depth could vary in an undesirable way. Placing medians as shown in Fig. 7 would provide support for the

chip cover. Here, the simulation was obtained using the same angles and specific-permeability ratio for those in Fig. 6. However, the wide, shallow section has been constructed with medians oriented parallel to the flow direction. If we assume that the inlet-channel width is 100 μm, then the expanded region will be 3-mm wide. The medians shown are then each 6.67-μm wide, such that the total width occupied is 53.3 μm (representing 1.8 percent of the channel width). For this example, the injected analyte band travels through the expanded region with negligible distortion caused by the presence of medians. This result is possible because the streaklines are parallel and straight—otherwise, dispersion would be introduced. The simulation of Fig. 7 also demonstrates that it is possible to contract the channel width back to its entrance value by placing faceted prisms symmetrically, as shown. Hence, point detection in a narrow exit—using laser-induced fluorescence, for example—is possible. Moreover, both line-of-sight optical absorption and laser-induced fluorescence can be combined for the channel of Fig. 7. This symmetric arrangement is always skew compensating, so the resulting six-interface system produces no net skew. For the simulation shown in Fig. 7, the length of the expanded section has been reduced to minimize the memory resources needed to perform the computation. In practice, the length of this section would be longer than that shown.

3.1 Flow Splitters, Manifolds, and Medians

Once a channel has been designed using faceted prisms, the resulting design can be copied and pasted in series or parallel to construct additional channel designs. For example, a flow displacer is drawn in Fig. 8 (a). The drawing of Fig. 8 (b) is constructed by placing a mirrored copy (flipped about a horizontal axis) side-by-side with the original. The line dividing the two objects separates sections of identical specific permeability, and the dividing line is parallel to the flow direction for each of the neighboring channel entrance sections. Because the flow is a potential flow, this wall can be treated as a streamline. As a result, the line dividing the upper and lower entrance sections of Fig. 8 (b) can be removed [58], yielding the flow splitter shown in Fig. 8 (c). The original channel design of Fig. 8 (a) features identical entrance and exit widths, resulting in two exit channels with half the entrance width in

Fig. 8 (c). A band that is injected into the channel with a material-line angle of zero is shown in the figure at time t_1. The band passes through the channel as shown at instances t_2, t_3, t_4, and t_5. As it flows in the direction indicated by the arrows, the band is divided in two by the splitter, and it exits with no material-line skew as it experiences diffusion broadening (for a Peclet number at the inlet of 46). It is also possible to design flow splitters with exit sections that are wider than the inlet by placing mirrored copies of a two-interface expander next to each other in an analogous manner to that shown in Fig. 8.

Electrokinetic flows can be divided into large numbers of channels using the faceted design method. The three-way splitter shown in Fig. 9 was constructed by placing three channels side-by-side, with the middle channel constructed using two zero-incidence-angle interfaces. The top channel was constructed using an incidence angle for Interface 1 of 5° while the corresponding incidence angle for the bottom channel is -5°. Channels can also be combined in series to produce intricate designs. For example, the channel of Fig. 10 was constructed by initially creating a five-way flow splitter from five channels placed in parallel. These channels, from the top to the bottom of the figure, have incidence angles for the first interface of 10°, 5°, 0°, -5°, and –10°. This five-way splitter is then copied, and the copy is flipped symmetrically about a vertical line and connected to the original splitter. The resulting channel splits the inlet flow into five channels, which then combine the flow back to a single exit channel, producing four dividing medians. These medians produce the minimum amount of dispersion for the injected band. Therefore, they are ideal for providing structural support for wide channels, and they can be placed within the wide section of a designed expander such as that shown in Fig. 5. The width of the medians can be increased by using larger incidence-angle increments for each of the five channels, and it is possible to construct a larger number of medians using the technique. When incorporated into a wide separation column, the resulting parallel channels will have reduced aspect ratios, potentially limiting the impact of transverse diffusion [18].

Two possible separation-column designs are shown in Fig. 11. The column of Fig. 11 (a) is similar to that shown in Fig. 5. An injection cross has been attached at the inlet, and the channel width is reduced at the exit and connected to a waste port. The same channel design is shown in Fig. 11 (b), except that

the length of the central region has been increased, and the designed median structure of Fig. 10 has been pasted into the wide, central section. The length of the medians has been increased to fill the length of the central channel.

Designs can have unintended consequences, as demonstrated in Fig. 12. Here, the simulation for the three-interface, skew-compensated expander of Fig. 5 has been repeated by decreasing the Peclet number by a factor of 10 (such that the inlet Peclet number is 39). This condition can be accomplished in practice by using a larger diffusivity or a smaller inlet velocity. As shown, this design results in a larger amount of diffusion broadening at the upper end of the channel, attributable to the longer path the top portion of the analyte band must travel in the third faceted prism before reaching the exit section. Therefore, line-of-sight, optical absorption measurements will yield signals that are spatially averaged from continuously varying analyte widths across the channel. For point detection at the channel exit, symmetric placement of prisms at the exit to contract the channel (back to the same width as the entrance section) will reduce this distance discrepancy. The relative effect can be minimized by lengthening the faceted prisms, such that the length discrepancy is reduced as a fraction of the total length of travel. Alternatively, additional interfaces can be employed to reduce the discrepancy in flow paths.

4. Summary, conclusions and recommendations

The results demonstrate the utility of faceted, multiple-interface systems. Multiple-interface designs can be obtained from iterative solution of simple, trigonometric equations. Skew-compensated designs can be constructed, resulting in wide channels in which bands travel with minimum dispersion. Alternatively, designs can produce band rotation purposely, thereby increasing the amount of channel expansion. The exit width of separation columns can be reduced to equal the inlet-channel width, allowing additional point detection at the exit port. Moreover, the designs are uncoupled completely: the interfaces are immune to the details of what passes before or after, as long as their compatibility conditions are satisfied locally. Therefore, the length of separation channels can be increased to fill the

available length on a chip substrate without changing the velocity distribution. Once an object has been constructed, the base object can be used in combination with identical copies or with other objects to produce flow splitters, manifolds, and medians. The length of the resulting objects can be increased, and the lengthened objects can then be pasted into the wide region of a separation channel to provide structural support and reduce the importance of transverse diffusion.

The uncertainty that results from practical considerations requires further study—both by modeling and by experimental tests. There are numerous manufacturing methods to produce abrupt variation in specific permeability, each contributing to hydrodynamic dispersion in a unique way. For example, if a simple, two-level etch is employed, dispersion will be introduced in the out-of-plane direction. This dispersion is minimized for comparatively shallow and wide channels. Such designs are highly amenable to common planar manufacturing techniques. Nevertheless, the physical limits of manufacturing will restrict the range of interface angles that can be implemented. Hence, the maximum expansion across a single interface is approached as the incident angle approaches the physically unrealizable value of 90°. The maximum achievable incidence angle will be determined by manufacturing methods. For example, the intersection of large-angle interfaces with channel walls will be eroded during wet-etching processes [88]. The degree of this erosion will be minimized for shallow-channel designs. Other manufacturing techniques do not suffer from the curved walls characteristic of wet etching, such as deep-reactive ion etching [83, 89], but the height-to-tilt ratio [83] will impact channel performance still. Surface roughness can also increase dispersion [90], an impact that is particularly important for extreme surface-to-volume ratios. Further study is necessary to evaluate the impact that such manufacturing issues have on the final system performance. It is also possible to increase the amount of expansion using smaller incidence angles and additional interfaces. For the wide, shallow channels considered, this approach requires use of five or seven interfaces. Because each interface will introduce dispersion, a practical upper bound on the number of interfaces will exist depending on the method used to vary the specific permeability of channel sections.

A number of methods can be used to select specific permeability, each resulting in different levels of dispersion [77]. For example, specific permeability could be chosen by alternating regions of open channel with regions filled with a porous packing material [28, 91-96]. Here, issues such as uniformity will require testing on faceted-interface performance. Moreover, local variations in zeta potential could depend on choice of packing materials [97], resulting in induced pressure gradients and band broadening [98, 99]. Choice of substrate material will also impact the performance of faceted interfaces. While separation channels designed using faceted interfaces should be ideal for construction from polymers [89, 100, 101]—therefore, enabling inexpensive, mass production—variations in surface properties [102, 103] could increase dispersion. Issues such as adsorption could also degrade performance of systems constructed to have a large surface-to-volume ratio [7, 104].

Acknowledgements

The authors thank Dahv Kliner, Sandia National Laboratories, for the discussions of on-chip absorption detection, and Boyd Wiedenman, Sandia National Laboratories, for the discussions of chip microfabrication. This work was supported financially by the Laboratory Directed Research and Development Program at Sandia National Laboratories. Sandia is a multiprogram laboratory operated by Sandia Corporation, a Lockheed-Martin company, for the United States Department of Energy under contract DE-AC04-94AL85000.

FIGURE CAPTIONS

Figure 1. Multi-interface channel diagram used to define nomenclature. (a) The channel widths, w_i, are defined by the length across the channel perpendicular to the direction of flow. The specific permeability is given by either σ_{sp1} (m^2) or σ_{sp2}, for the bipermeability systems considered in this paper. (b) An injected band is shown for six instances denoted by t_i. The material-line angles ψ_i are defined as the angle between the direction of flow and the normal to the material line.

Figure 2. Plot of the incidence angle for the second interface, $\theta_{21,}$ of a three-interface, skew-compensated system versus the incidence angle for the first and third interfaces. Each curve corresponds to a distinct permeability ratio: (a) Full range of angles, and (b) close-up of large incidence angles for interfaces 1 and 3.

Figure 3. (a) Plot of the expansion ratio for a three-interface, skew compensated system. (b) The expansion ratio is divided by the value produced by the first or third interface.

Figure 4. Plot of the overall flow turning angle for a skew-compensated, three-interface system. Figures 2-4 demonstrate the simple design curves used for the channels modeled in this paper.

Figure 5. Numerical simulation of flow in a three-interface, skew-compensated expander for a specific permeability ratio $\sigma_{sp1}/\sigma_{sp2}$ of 10. (a) The direction of flow is indicated by the black arrows along the upper wall of the channel. The relative speed is indicated by the color table in the upper left corner of the figure. The incidence angles θ_1, θ_{21}, and θ_{31} have values of 85°, 22.82°, and –85°, respectively, resulting in overall expansion and turning-angle values of 14.32 and 53.8094°, respectively. (b) Solution for the identical channel showing the location of an injected analyte band at times t_i. The expanded length of the channel in the direction parallel to the material line is ideal for line-of-sight optical absorption measurements, as indicated by the position of the laser and photodetector. The unetched substrate is indictated by the gray region.

Figure 6. Numerical simulation of flow in a three-interface expander for which the incidence angles angles θ_1, θ_{21}, and θ_{31} have values of 81.1689°, 0°, and -81.1689°, respectively. The permeability ratio is 10. The material line angle in the expanded exit section is ψ_6=55.44°. The overall expansion ratio is 30, and the overall turning angle is 0°. The Peclet number at the inlet is ~200.

Figure 7. Simulation of a three-interface expander for interface angles identical to those for the simulation of Fig. 6, demonstrating the placement of eight rectangular medians in the expanded section parallel to the direction of flow. The three sequential faceted prisms at the inlet have been pasted symmetrically at the opposite side of the expanded region to shrink the channel width back to that of the channel inlet, demonstrating the possibility of point detection at the exit.

Figure 8. Illustration of the process used to construct a two-way flow splitter using faceted prisms. (a) A two-interface displacer is placed next to its mirror copy with the entrance sections aligned as shown in (b). The line dividing the two entrance sections in (b) is removed, resulting in the splitter simulated in (c).

Figure 9. Demonstration of a faceted, three-way flow splitter constructed using a process similar to that shown in the illustration of Fig. 8.

Figure 10. Demonstration of electrokinetic flow behavior for four engineered medians with a specific-permeability ratio of 10. Here, a five-way splitter is constructed in a fashion identical to the three-way splitter of Fig. 10. The resulting five-way splitter is then mirrored along a vertical line, and pasted in series to recombine the five channels. The four lengths of unetched substrate dividing the channels can be used as medians for structural support. Median width can be increased by using larger incidence-angle displacers, or by increasing the length of sections in which the specific permeability is denoted by σ_{sp2}. Median length can be increased by increasing the length of the central section with specific permeability σ_{sp1}. Similar median structures can be designed for inlet an exit sections with specific permeability σ_{sp2}.

Figure 11. Illustration demonstrating the layout of separation columns based on the three-interface, skew-compensated system of Fig. 5. An injection cross with three solution ports has been connected at the channel inlet, and a waste port has been connected at the channel exit. The upper channel (a) has an open expanded shallow region, while the lower channel (b) had been extended and medians—constructed using a five-way flow splitter (Fig. 11)—have been pasted within the channel.

Figure 12. Simulation of the three-interface, skew-compensated expander of Fig. 5 for a Peclet number that has been decreased by an order of magnitude. The degree of band broadening owing to diffusion is observed to be larger on the top of the channel.

References

[1] J. W. Jorgenson, K. D. Lukacs, Anal. Chem. 53 (1981) 1298-1302.

[2] J. H. Knox, Chromatographia 26 (1988) 329-337.

[3] J. H. Knox, K. A. McCormack, Chromatographia 38 (1994) 207-214.

[4] J. H. Knox, K. A. McCormack, Chromatographia 38 (1994) 215-221.

[5] B. X. Mayer, J. Chromatogr. A 907 (2001) 21-37.

[6] C. A. Monnig, J. W. Jorgenson, Anal. Chem. 63 (1991) 802-807.

[7] R. J. Nelson, A. Paulus, A. S. Cohen, A. Guttman, B. L. Karger, J. Chromatogr. 480 (1989) 111-127.

[8] A. Vinther, H. Soeberg, J. Chromatogr. 559 (1991) 27-42.

[9] Y. J. Xue, E. S. Yeung, Anal. Chem. 66 (1994) 3575-3580.

[10] R. O. Cole, D. L. Hiller, C. A. Chwojdak, M. J. Sepaniak, J. Chromatogr. A 736 (1996) 239-245.

[11] L. M. Mosulishvili, V. A. Barnov, N. Y. Tsibakhashvili, H. Engelhardt, W. Beck, J. Anal. Chem. 56 (2001) 512-514.

[12] A. Cifuentes, H. Poppe, Electrophoresis 16 (1995) 2051-2059.

[13] A. Cifuentes, M. A. Rodriguez, F. J. Garcia-Montelongo, J. Chromatogr. A 737 (1996) 243-253.

[14] A. Cifuentes, X. Xu, W. T. Kok, H. Poppe, J. Chromatogr. A 716 (1995) 141-156.

[15] M. Jansson, A. Emmer, J. Roeraade, J. High Resolut. Chromatogr. 12 (1989) 797-807.

[16] T. Tsuda, J. V. Sweedler, R. N. Zare, Anal. Chem. 62 (1990) 2149-2152.

[17] B. Gas, M. Stedry, E. Kenndler, Electrophoresis 18 (1997) 2123-2133.

[18] X. Zhang, F. E. Regnier, J. Chromatogr. A 869 (2000) 319-328.

[19] K. D. Bartle, P. Myers, J. Chromatogr. A 916 (2001) 3-23.

[20] Z. H. Fan, D. J. Harrison, Anal. Chem. 66 (1994) 177-184.

[21] D. J. Harrison, A. Manz, Z. H. Fan, H. Ludi, H. M. Widmer, Anal. Chem. 64 (1992) 1926-1932.

[22] S. C. Jacobson, C. T. Culbertson, J. E. Daler, J. M. Ramsey, Anal. Chem. 70 (1998) 3476-3480.

[23] K. Seiler, D. J. Harrison, A. Manz, Anal. Chem. 65 (1993) 1481-1488.

[24] K. Swinney, D. J. Bornhop, Electrophoresis 23 (2002) 613-620.

[25] H. Salimi-Moosavi, Y. T. Jiang, L. Lester, G. McKinnon, D. J. Harrison, Electrophoresis 21 (2000) 1291-1299.

[26] D. Ross, M. Gaitan, L. E. Locascio, Anal. Chem. 73 (2001) 4117-4123.

[27] R. F. Probstein, Physicochemical Hydrodynamics, Wiley-Interscience, New York, NY, 1994.

[28] P. A. Greenwood, G. M. Greenway, Trac-Trends Anal. Chem. 21 (2002) 726-740.

[29] P. D. I. Fletcher, S. J. Haswell, V. N. Paunov, Analyst 124 (1999) 1273-1282.

[30] H. J. Crabtree, E. C. S. Cheong, D. A. Tilroe, C. J. Backhouse, Anal. Chem. 73 (2001) 4079-4086.

[31] D. Q. Li, Colloid Surf. A-Physicochem. Eng. Asp. 195 (2001) 35-57.

[32] C. Yang, D. Q. Li, J. H. Masliyah, Int. J. Heat Mass Transfer 41 (1998) 4229-4249.

[33] C. Yang, D. Q. Li, Colloid Surf. A-Physicochem. Eng. Asp. 143 (1998) 339-353.

[34] G. M. Mala, D. Q. Li, J. D. Dale, Int. J. Heat Mass Transfer 40 (1997) 3079-3088.

[35] L. Q. Ren, D. Q. Li, W. L. Qu , J. Colloid Interface Sci. 233 (2001) 12-22.

[36] K. B. Mogensen, N. J. Petersen, J. Hubner, J. P. Kutter, Electrophoresis 22 (2001) 3930-3938.

[37] N. J. Petersen, K. B. Mogensen, J. P. Kutter, Electrophoresis 23 (2002) 3528-3536.

[38] K. B. Mogensen, P. Friis, J. Hubner, N. Petersen, A. M. Jorgensen, P. Tellemen, J. P. Kutter, Opt. Lett. 26 (2001) 716-718.

[39] P. Friis, K. Hoppe, O. Leistiko, K. B. Mogensen, J. Hubner, J. P. Kutter, Appl. Optics 40 (2001) 6246-6251.

[40] B. G. Splawn, F. E. Lytle, Anal. Bioanal. Chem. 373 (2002) 519-525.

[41] S. Z. Qi, X. Z. Liu, S. Ford, J. Barrows, G. Thomas, K. Kelly, A. McCandless, K. Lian, J. Goettert, S. A. Soper, Lab Chip 2 (2002) 88-95.

[42] R. M. Tiggelaar, T. T. Veenstra, R. G. P. Sanders, J. G. E. Gardeniers, M. C. Elwenspoek, A. van den Berg, Talanta 56 (2002) 331-339.

[43] G. Pandraud, T. M. Koster, C. Gui, M. Dijkstra, A. van den Berg, P. V. Lambeck, Sens. Actuator A-Phys. 85 (2000) 158-162.

[44] G. L. Duveneck, M. A. Bopp, M. Ehrat, M. Haiml, U. Keller, M. A. Bader, G. Marowsky, S. Soria, Appl. Phys. B-Lasers Opt. 73 (2001) 869-871.

[45] P. N. Zeller, G. Voirin, R. E. Kunz, Biosens. Bioelectron. 15 (2000) 591-595.

[46] J. Kruger, K. Singh, A. O'Neill, C. Jackson, A. Morrison, P. O'Brien, J. Micromech. Microeng. 12 (2002) 486-494.

[47] O. Hofmann, G. Voirin, P. Niedermann, A. Manz, Anal. Chem. 74 (2002) 5243-5250.

[48] R. A. Potyrailo, S. E. Hobbs, G. M. Hieftje, Fresenius J. Anal. Chem. 362 (1998) 349-373.

[49] M. L. Chabinyc, D. T. Chiu, J. C. McDonald, A. D. Stroock, J. F. Christian, A. M. Karger, G. M. Whitesides, Anal. Chem. 73 (2001) 4491-4498.

[50] Z. H. Liang, N. Chiem, G. Ocvirk, T. Tang, K. Fluri, D. J. Harrison, Anal. Chem. 68 (1996) 1040-1046.

[51] S. C. Jacobson, R. Hergenroder, L. B. Koutny, R. J. Warmack, J. M. Ramsey, Anal. Chem. 66 (1994) 1107-1113.

[52] E. Verpoorte, Electrophoresis 23 (2002) 677-712.

[53] M. Vazquez, G. McKinley, L. Mitnik, S. Desmarais, P. Matsudaira, D. Ehrlich, J. Chromatogr. B 779 (2002) 163-171.

[54] C. A. Emrich, H. J. Tian, I. L. Medintz, R. A. Mathies, Anal. Chem. 74 (2002) 5076-5083.

[55] R. J. Yang, L. M. Fu, G. B. Lee, J. Sep. Sci. 25 (2002) 996-1010.

[56] E. Zubritsky, Anal. Chem. 72 (2000) 687A-690A.

[57] B. Gas, E. Kenndler, Electrophoresis 23 (2002) 3817-3826.

[58] S. K. Griffiths, R. H. Nilson, Anal. Chem. 73 (2001) 272-278.

[59] J. I. Molho, A. E. Herr, B. P. Mosier, J. G. Santiago, T. W. Kenny, R. A. Brennen, G. B. Gordon, B. Mohammadi, Anal. Chem. 73 (2001) 1350-1360.

[60] A. Manz, L. Bousse, A. Chow, T. B. Metha, A. Kopf-Sill, J. W. Parce, Fresenius J. Anal. Chem. 371 (2001) 195-201.

[61] B. M. Paegel, L. D. Hutt, P. C. Simpson, R. A. Mathies, Anal. Chem. 72 (2000) 3030-3037.

[62] I. L. Medintz, B. M. Paegel, R. A. Mathies, J. Chromatogr. A 924 (2001) 265-270.

[63] I. L. Medintz, B. M. Paegel, R. G. Blazej, C. A. Emrich, L. Berti, J. R. Scherer, R. A. Mathies, Electrophoresis 22 (2001) 3845-3856.

[64] B. M. Paegel, C. A. Emrich, G. J. Weyemayer, J. R. Scherer, R. A. Mathies, Proc. Natl. Acad. Sci. USA 99 (2002) 574-579.

[65] B. M. Paegel, S. H. I. Yeung, R. A. Mathies, Anal. Chem. 74 (2002) 5092-5098.

[66] B. M. Paegel, R. G. Blazej, R. A. Mathies, Curr. Opin. Biotechnol. 14 (2003) 42-50.

[67] A. R. Kopf-Sill, J. W. Parce, Microfluidic Systems Incorporating Varied Channel Dimensions, US Patent 5842787, 1998.

[68] L. M. Fu, R. J. Yang, G. B. Lee, Electrophoresis 23 (2002) 602-612.

[69] E. S. Nordman, Serpentine Channel with Self-Correcting Bends, US Patent 6176991, 2001.

[70] S. K. Griffiths, R. H. Nilson, Anal. Chem. 74 (2002) 2960-2967.

[71] N. Gottschlich, S. C. Jacobson, C. T. Culbertson, J. M. Ramsey, Anal. Chem. 73 (2001) 2669-2674.

[72] C. T. Culbertson, S. C. Jacobson, J. M. Ramsey, Anal. Chem. 72 (2000) 5814-5819.

[73] C. T. Culbertson, S. C. Jacobson, J. M. Ramsey, Anal. Chem. 70 (1998) 3781-3789.

[74] D. Dutta, D. T. Leighton, Anal. Chem. 74 (2002) 1007-1016.

[75] T. J. Johnson, D. Ross, M. Gaitan, L. E. Locascio, Anal. Chem. 73 (2001) 3656-3661.

[76] R. Qiao, N. R. Aluru, Sens. Actuator A-Phys. 104 (2003) 268-274.

[77] G. J. Fiechtner, E. B. Cummings, Anal. Chem., in press (2003).

[78] B. H. Weigl, P. Yager, Science 283 (1999) 346-347.

[79] B. H. Weigl, R. L. Bardell, C. R. Cabrera, Adv. Drug Deliv. Rev. 55 (2003) 349-377.

[80] P. Jandik, B. H. Weigl, N. Kessler, J. Cheng, C. J. Morris, T. Shulte, N. Avdalovic, J. Chromatogr. A 954 (2002) 33-40.

[81] C. L. Colyer, S. D. Mangru, D. J. Harrison, J. Chromatogr. A 781 (1997) 271-276.

[82] L. Bousse, S. Mouradian, A. Minalla, H. Yee, K. Williams, R. Dubrow, Anal. Chem. 73 (2001) 1207-1212.

[83] B. He, N. Tait, F. E. Regnier, Anal. Chem. 70 (1998) 3790-3797.

[84] H. P. Chou, C. Spence, A. Scherer, S. Quake, Proc. Natl. Acad. Sci. USA 96 (1999) 11-13.

[85] E. B. Cummings, S. K. Griffiths, R. H. Nilson, P. H. Paul, Anal. Chem. 72 (2000) 2526-2532.

[86] E. B. Cummings, S. K. Griffiths, R. H. Nilson, Applied Microfluidic Physics LDRD Final Report, Sandia National Laboratories, Livermore, CA, 2001, SAND 2002-8018, pp. 65-93.

[87] G. J. Fiechtner, E. B. Cummings, Proc. MicroTAS, in press (2003).

[88] T. McCreedy, Trac-Trends Anal. Chem. 19 (2000) 396-401.

[89] N. Giordano, J. T. Cheng, J. Phys.-Condens. Matter 13 (2001) R271-R295.

[90] Q. S. Pu, R. Luttge, H. J. G. E. Gardeniers, A. van den Berg, Electrophoresis 24 (2003) 162-171.

[91] R. K. Marcus, W. C. Davis, B. C. Knippel, L. LaMotte, T. A. Hill, D. Perhia, J. D. Jenkins, J. Chromatogr. A 986 (2003) 17-31.

[92] D. J. Throckmorton, T. J. Shepodd, A. K. Singh, Anal. Chem. 74 (2002) 784-789.

[93] A. Deneanu, G. S. Chirica, V. T. Remcho, J. Sep. Sci. 25 (2002) 1252-1256.

[94] K. Morishima, B. D. Bennett, M. T. Dulay, J. P. Quirino, R. N. Zare, J. Sep. Sci. 25 (2002) 1226-1230.

[95] L. A. Colon, T. D. Maloney, A. M. Fermier, J. Chromatogr. A 887 (2000) 43-53.

[96] J. H. Knox, I. H. Grant, Chromatographia 32 (1991) 317-328.

[97] A. S. Rathore, K. J. Reynolds, L. A. Colon, Electrophoresis 23 (2002) 2918-2928.

[98] A. E. Herr, J. I. Molho, J. G. Santiago, M. G. Mungal, T. W. Kenny, M. G. Garguilo, Anal. Chem. 72 (2000) 1053-1057.

[99] V. P. Andreev, S. G. Dubrovsky, Y. V. Stepanov, J. Microcolumn Sep. 9 (1997) 443-450.

[100] O. Rotting , W. Ropke, H. Becker, C. Gartner, Microsyst. Technol. 8 (2002) 32-36.

[101] H. Becker, C. Gartner, Electrophoresis 21 (2000) 12-26.

[102] D. Ross, T. J. Johnson, L. E. Locascio, Anal. Chem. 73 (2001) 2509-2515.

[103] X. Q. Ren, M. Bachman, C. Sims, G. P. Li, N. Allbritton, J. Chromatogr. B 762 (2001) 117-125.

[104] J. K. Towns, F. E. Regnier, Anal. Chem. 64 (1992) 2473-2478.

Figures

Fiechtner and Cummings

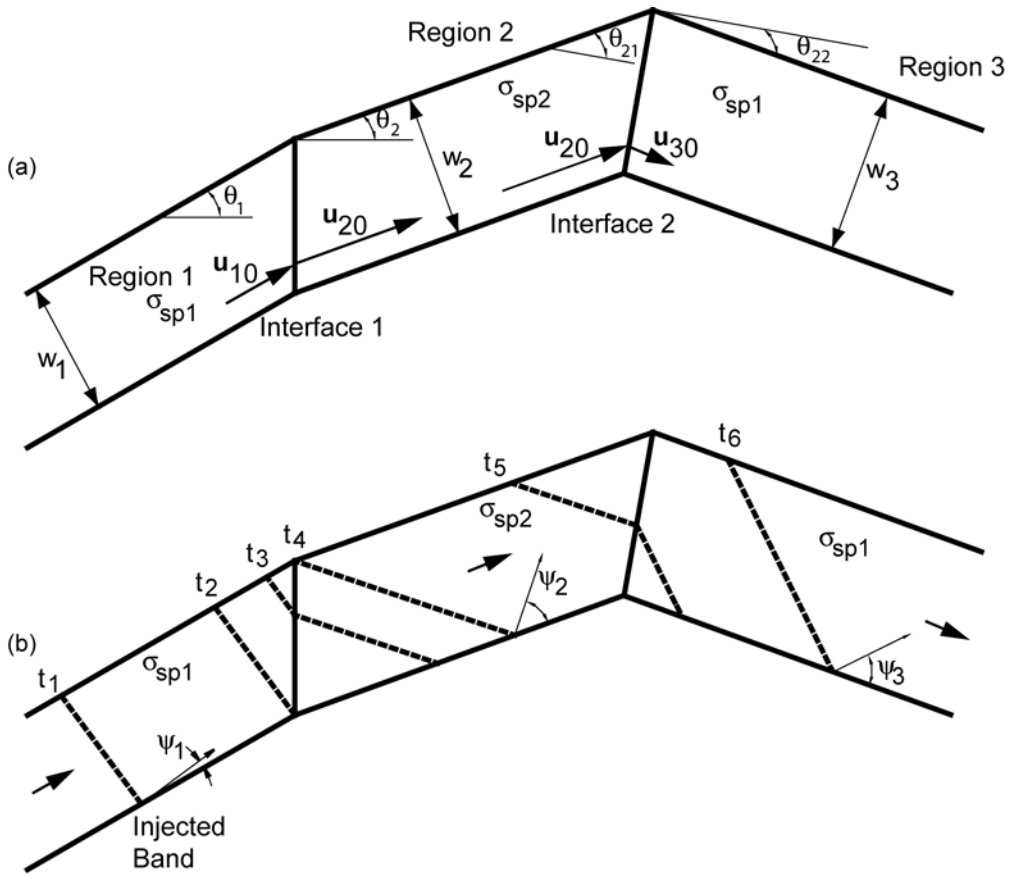

Figure 1 (Fiechtner and Cummings)

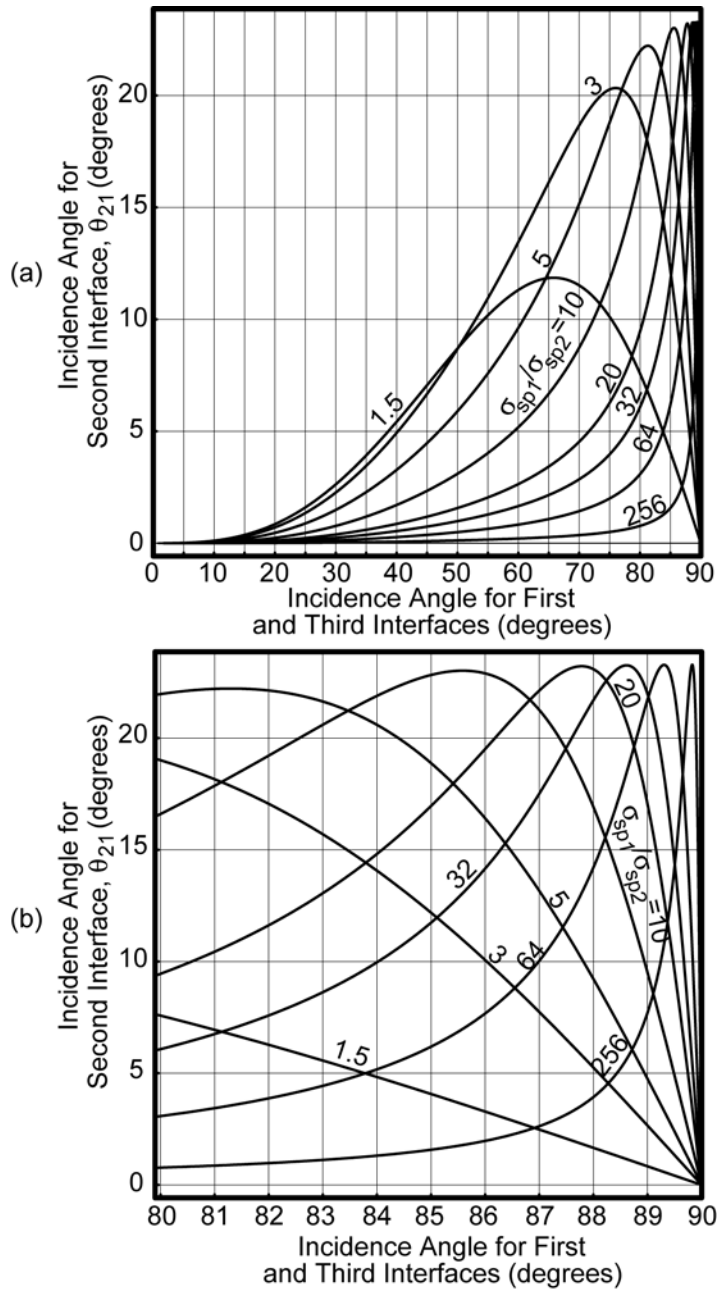

Figure 2 (Fiechtner and Cummings)

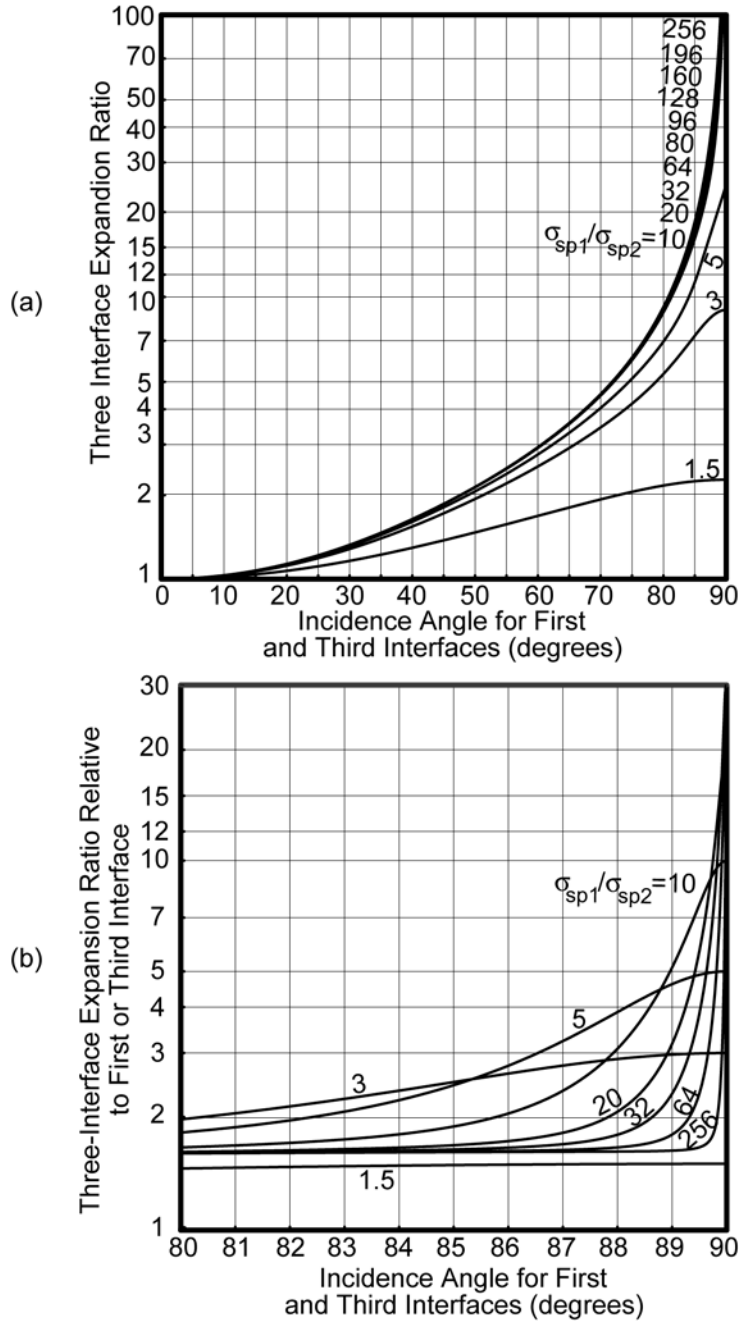

Figure 3 (Fiechtner and Cummings)

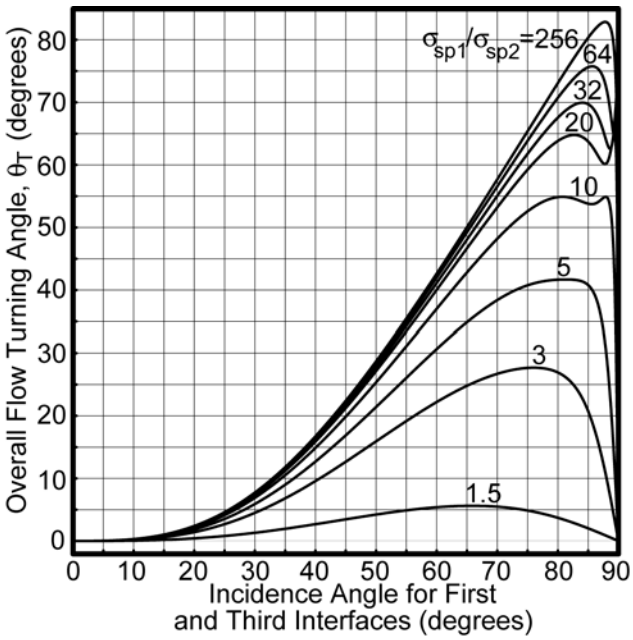

Figure 4 (Fiechtner and Cummings)

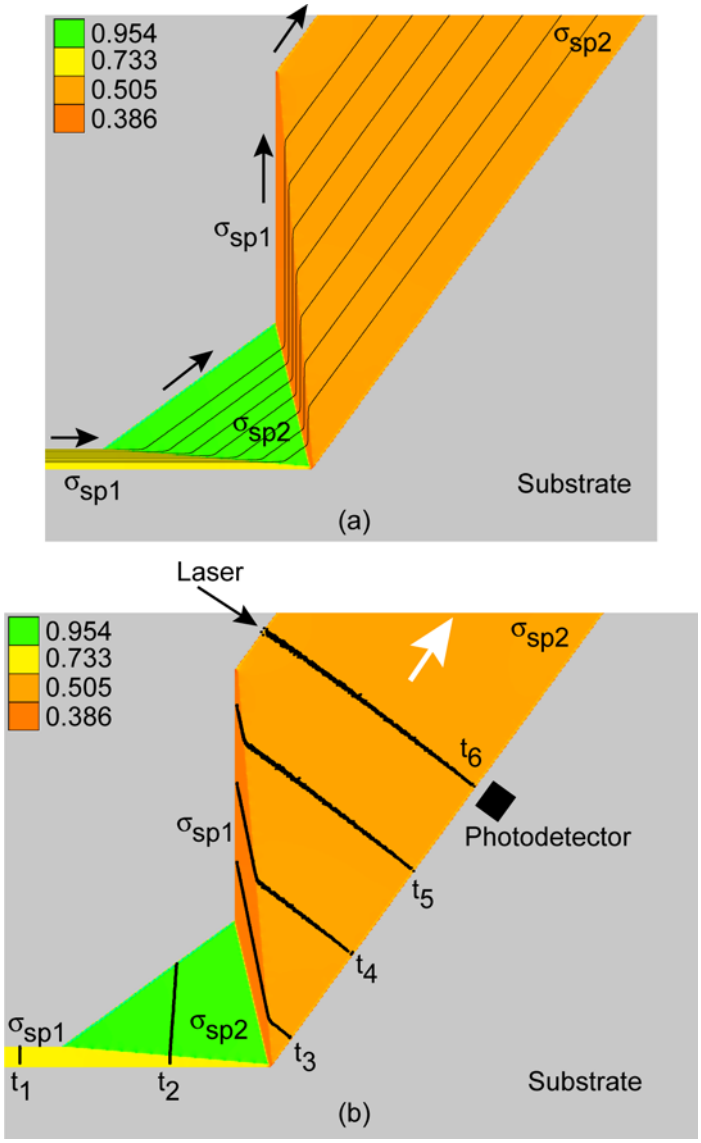

Figure 5 (Fiechtner and Cummings)

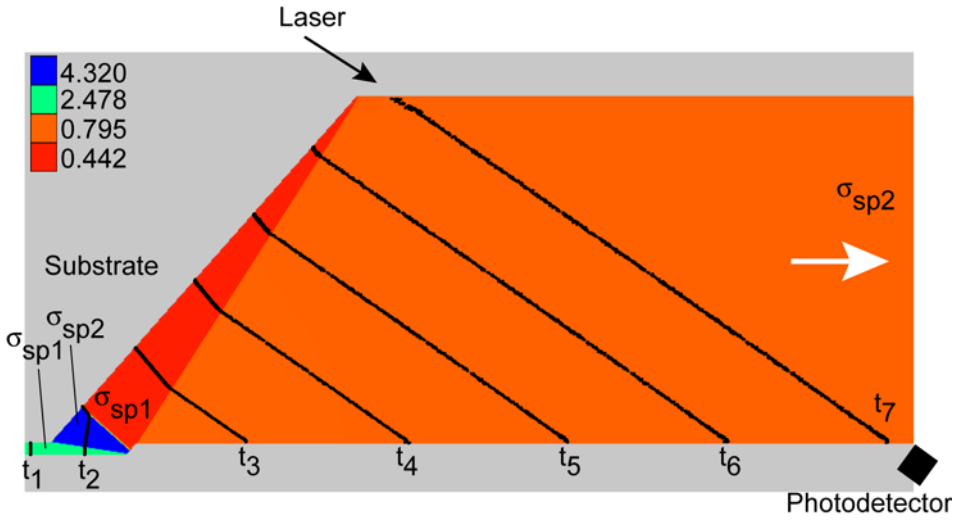

Figure 6 (Fiechtner and Cummings)

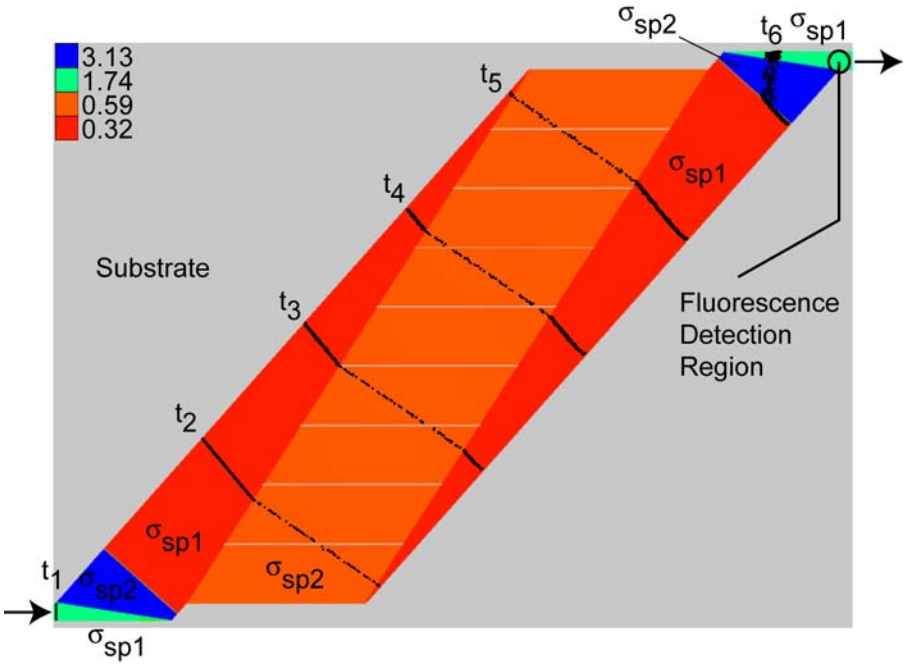

Figure 7 (Fiechtner and Cummings)

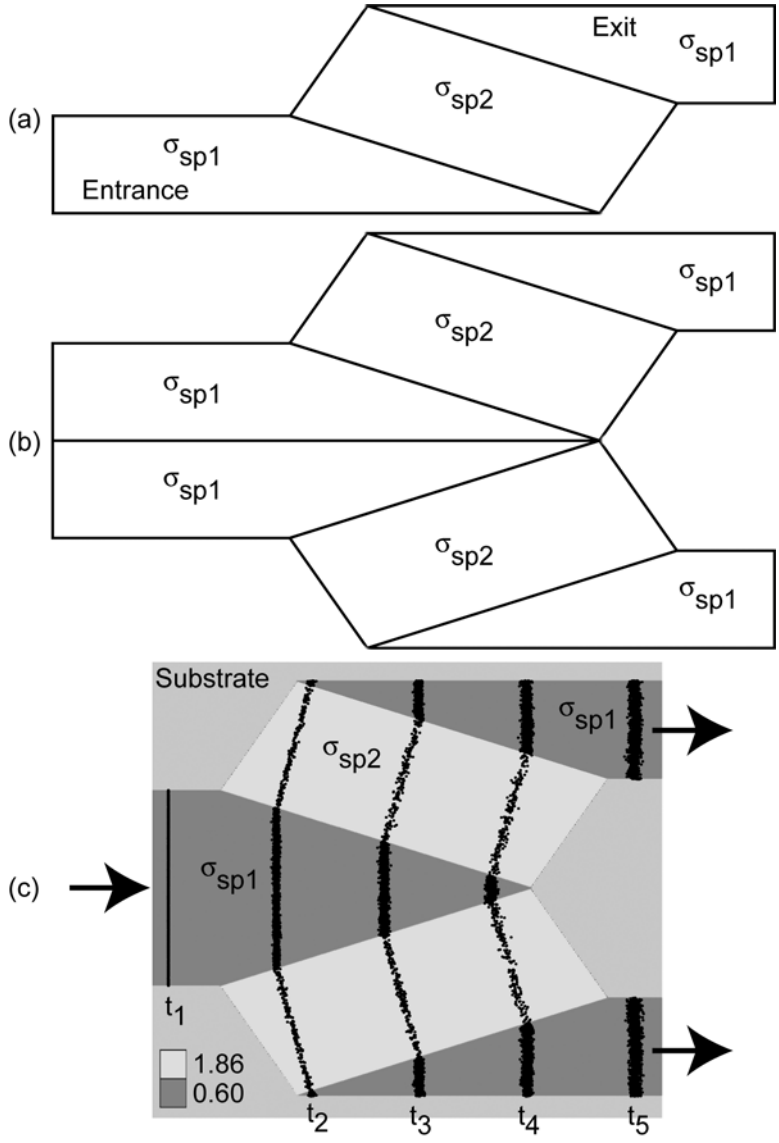

Figure 8 (Fiechtner and Cummings)

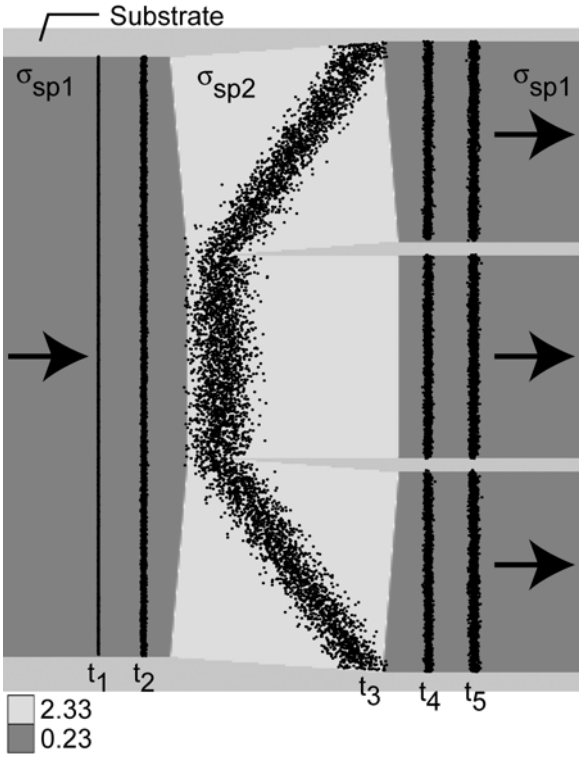

Figure 9 (Fiechtner and Cummings)

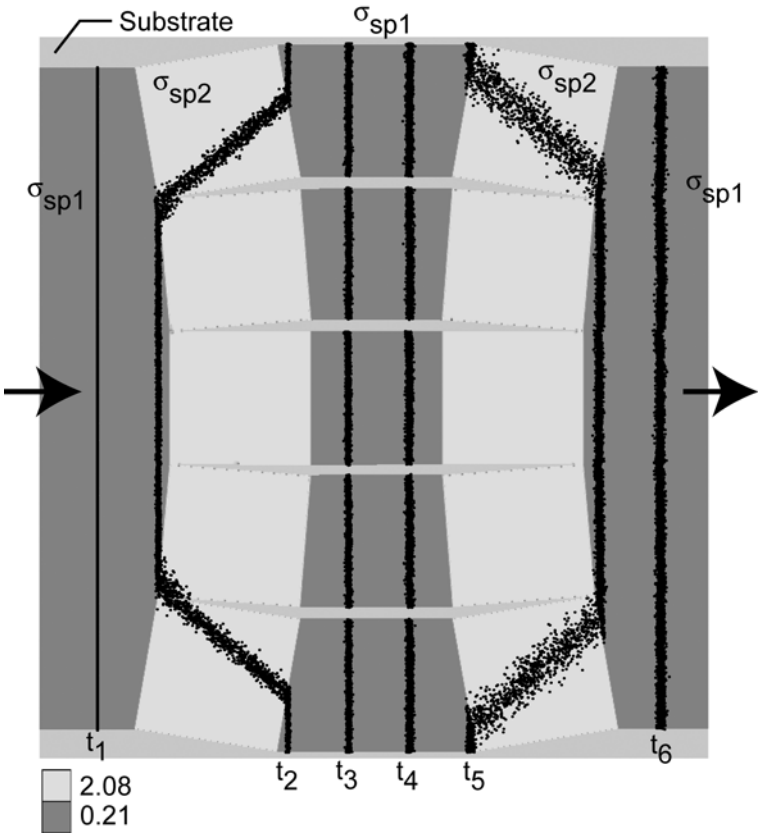

Figure 10 (Fiechtner and Cummings)

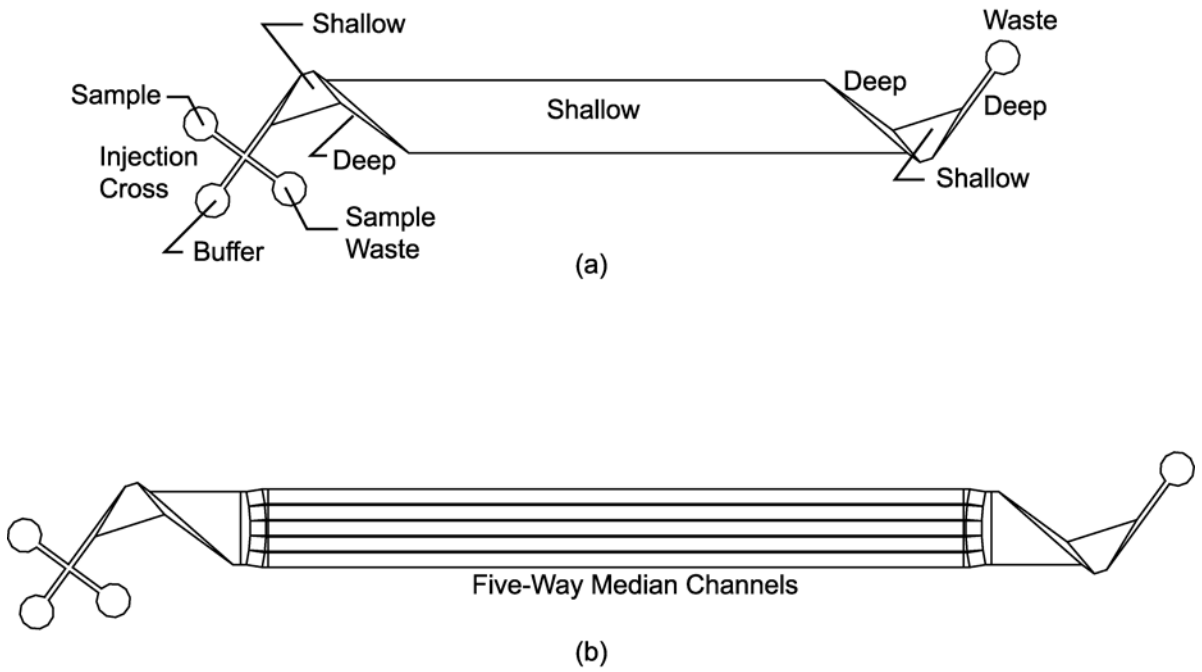

Figure 11 (Fiechtner and Cummings)

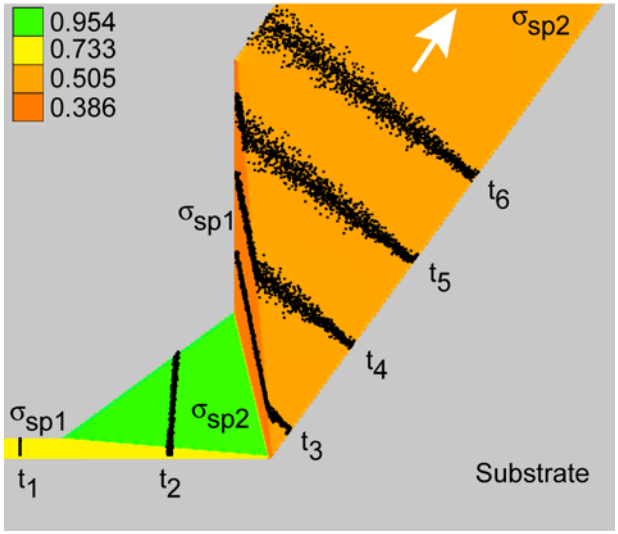

Figure 12 (Fiechtner and Cummings)